Available online at www.sciencedirect.com
ScienceDirect
Journal of Power Sources 174 (2007) 735–740
JOURNAL OF POWER SOURCES
www.elsevier.com/locate/jpowsour

Short communication

Mixed layered Ni–Mn–Co hydroxides: Crystal structure, electronic state of ions, and thermal decomposition

N.V. Kosova [a,*], E.T. Devyatkina [a], V.V. Kaichev [b]

[a] *Institute of Solid State Chemistry and Mechanochemistry, SB RAS, ul. Kutateladze 18, 630128 Novosibirsk, Russia*
[b] *Boreskov' Institute of Catalysis, SB RAS, pr. Acad. Lavrent' eva 5, 630090 Novosibirsk, Russia*

Available online 27 June 2007

Abstract

It has been shown that varying conditions of co-precipitation processes, two types of mixed Ni–Mn–Co hydroxides: either brucite, or hydrotalcite-like (LDHs)—with different Ni/Mn/Co ratio can be prepared. According to XPS study, these hydroxides are mixed-valence materials: Ni ions present in 2+ oxidation state, whereas Mn and Co ions are in 3+/4+ and 2+/3+ state, respectively; their oxidation state increases with an increase of their content in hydroxides. For Ni-rich hydroxides, a strong effect of nickel segregation is observed indicating that chemistry of the surface and of the bulk is different. Mixed Ni–Mn–Co hydroxides decompose in two steps resulting in formation of NiO bunsenite and $(Ni,Co,Mn)_3O_4$ spinel.

Keywords: Ni–Co–Mn layered hydroxides; LDHs; Mixed-valence materials; Crystal structure; XPS; Thermal decomposition

1. Introduction

Nickel hydroxide is well known as a positive electrode material for Ni-based alkaline secondary cells. It exists in two polymorphic modifications: β (brucite-like) and α (hydrotalcite-like), the latter referred to layered double hydroxides (LDHs). α-$Ni(OH)_2$ is characterized by an increased interlayer distance: 7.6 Å instead of 4.6 Å observed in β-nickel hydroxide [1,2]. Stabilization of α-nickel hydroxide is achieved by increasing isomorphous substitution of Ni^{2+} with a suitable trivalent cation M^{3+} to yield a layer composition of $[Ni^{2+}{}_{1-x}M^{3+}{}_x(OH)_2]^{x+}$. Different anions are intercalated in the interslab space for charge compensation and stability. A variety of Ni-based LDHs with Me^{3+} ions such as Al [3], Co [4], Fe [5], and Cr [6] has been studied. But only a few papers reported on hydrotalcite-like Ni hydroxide containing manganese [7–9]. It is well known that manganese in alkaline medium can exist in either Mn^{3+} or Mn^{4+} states. Mn^{3+} (d^4) ions in LDHs are present in the high spin state since hydroxyl ions act as weak field ligands. High spin d^4 systems are susceptible to Jahn-Teller distortion, a factor that introduces lattice instability in the LDHs. This lattice instability can be overcome, e.g., by oxidation of Mn^{3+} to Mn^{4+}. However, according to [6], tetravalent ions can be introduced in very small amounts ($x \sim 0.01$). The main difficulty in incorporating M^{4+} ions in the LDHs is the enhanced cation–cation repulsions with monovalent hydroxyl ions. In such an event, the hydroxyl ions lose protons and turn into oxide ions, which on account of their higher negative charge can accommodate M^{4+} cations [6]. In the LDHs of Ni with Mn, partial proton loss results in a phase with the composition $Ni^{2+}{}_{1-x}Mn^{4+}{}_x(OH)_{2-2x}(O)_{2x}\cdot yH_2O$. This can also be formulated as a composite $(1-x)Ni(OH)_2\cdot xMnO_2\cdot yH_2O$. According to previous study [7,8], the ageing of α-$Ni_{1-x}Mn_x(OH)_2$ in the KOH medium leads to spontaneous oxidation of the Mn^{3+} to Mn^{4+} ions and a formation of interstratified structure (for $x \geq 0.2$) which includes α- and β-domains along *c*-axis related to fluctuations of the manganese distribution within the slabs. On the other hand, the authors [10] published the hydrothermal synthesis of a series of $Ni(OH)_2$–manganese oxide compounds with a mixed layered structure by inserting nickel hydroxide into layered manganese oxides, Na- and Ni-birnessite. Their structure is similar to manganese oxide minerals – asbolanes – with incontinuous metal hydroxide layers, such as $Ni(OH)_2$, CoOOH or $Co(OH)_3$, $Mn(OH)_2$, and $Cu(OH)_2$ in the interlayer spaces of layered manganese oxide (see ASTM 43-1459).

Hydrotalcite-like compounds as well as the products obtained by their thermal treatment have found many practical applications such as catalysts or catalyst precursors, ion exchangers, adsorbents, and polymer stabilizers [9]. Recently, an interest to mixed Ni-based hydroxides arouse due to their use as reagents

* Corresponding author. Tel.: +7 383 3363843; fax: +7 383 3322847.
E-mail address: kosova@solid.nsc.ru (N.V. Kosova).

0378-7753/$ – see front matter © 2007 Elsevier B.V. All rights reserved.
doi:10.1016/j.jpowsour.2007.06.109

for the synthesis of a new generation of layered cathode materials – $LiNi_{1-x-y}Mn_xCo_yO_2$ – for rechargeable lithium batteries [11–16]. However, we have found only a few papers on mixed Ni–Co–Mn hydroxides [17,18].

The aim of the present study was to investigate crystal structure and electronic states of ions in mixed Ni–Mn–Co hydroxides synthesized by co-precipitation method under different conditions and with variable Ni/Mn/Co ratio as well as their thermal decomposition.

2. Experimental

Mixed Ni–Mn–Co precipitates with atomic ratio Ni/Mn/Co = 0.8/0.1/0.1; 0.6/0.2/0.2 and 0.33/0.33/0.33 were prepared by standard aqueous co-precipitation method. For one series, alkaline solutions of NH_4OH and NaOH were rapidly added to mixed solutions of Ni^{2+}, Mn^{2+} and Co^{2+} sulphates with stirring under argon atmosphere. For another series, mixed solutions of Ni^{2+}, Mn^{2+} and Co^{2+} nitrates were added dropwise to alkaline solutions of Na_2CO_3 and NaOH in air. In the latter case, H_2O_2 was added to oxidize Me^{2+} ions to higher oxidation states. The pH was controlled to be 10–11. The precipitates change in color from greenish-blue to brown during the synthesis. The color of the samples becomes darker with an increased Mn content. The resulting precipitates were aged and then collected by centrifugation. The solid products were washed with distilled water several times and dried at 60–80 °C in air. The samples prepared in argon from sulphates will be referred below as *samples A* and those prepared from nitrates in air as *samples B*.

Powder X-ray diffraction (XRD) patterns were recorded on a DRON-3M diffractometer, using Cu Kα irradiation; 2θ angle ranged from 4° to 70°; a step size of 0.02°. Fourier transformed infrared (FTIR) spectra of the pellets with CsI were recorded on a FTIR-spectrometer (Bruker) in the 200–4000 cm^{-1} range. Thermogravimetric (TG) and differential thermal analysis (DTA) curves were recorded on a MOM derivatograph (Hungary) in air at a rate of 10° min^{-1} in the temperature range 25–1000 °C. X-ray photoelectron spectroscopy (XPS) data were obtained by a VG ESCALAB HP spectrometer using non-monochromatized Al Kα radiation ($h\nu = 1486.6$ eV). Chemical analysis was performed by inductively coupled plasma (ICP) emission spectroscopy.

3. Results and discussion

3.1. Chemical analysis

The results of chemical analysis of as prepared hydroxides are presented in Table 1. They show that Ni/Mn/Co ratios well correlate with those of initial solutions. It is confirmed by the fact that filtrates were colorless, while the initial salt solutions before precipitation were colored. Chemical analysis shows no traces of Ni, Co or Mn in filtrates.

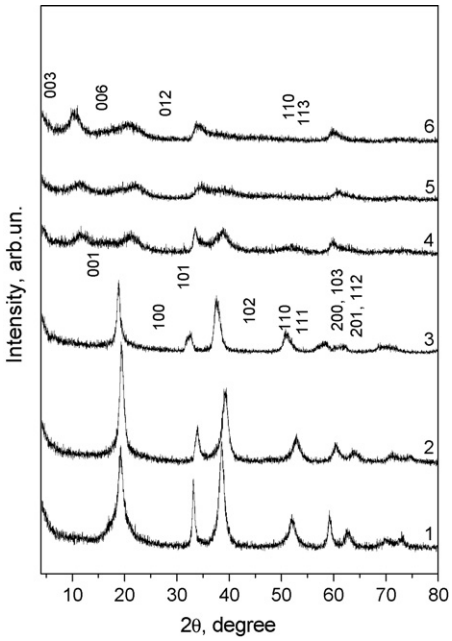

Fig. 1. X-Ray patterns of as prepared mixed Ni–Mn–Co hydroxides: 1, 4: $Ni_{0.8}/Mn_{0.1}/Co_{0.1}$; 2, 5: $Ni_{0.6}/Mn_{0.2}/Co_{0.2}$; 3, 4: $Ni_{0.33}/Mn_{0.33}/Co_{0.33}$; 1–3: *samples A*; 4–6: *samples B*.

3.2. Crystal and local structure

According to XRD patterns shown in Fig. 1, all as prepared *samples A* have a layered hexagonal structure almost consistent to the typical fingerprint of β-$M(OH)_2$ (M = Ni, Co, Mn) structure and are well indexed in *P*-3*m*1 space group. The absence of impurity phases (e.g., MnO_2) in X-ray patterns of as prepared hydroxides indicates that Ni, Co and Mn are homogeneously distributed within the particles. The broad peaks are believed to be a result of both small crystal size and microstrains. Lattice parameters are present in Table 1. It is known that ionic radius increases in the row Ni^{2+}–Co^{2+}–Mn^{2+} in octahedral coordination. However, for as prepared $Ni_{0.8}/Co_{0.1}/Mn_{0.1}$ and $Ni_{0.6}/Co_{0.2}/Mn_{0.2}$ samples, parameter *a* is even lower than for pure β-$Ni(OH)_2$. This points Mn to be incorporated into the structure with an oxidation state higher than 2+. On the other hand, *samples B* are poorly crystallized. The overall aspect of diffractograms indicates a layered structure, similar to hydrotalcite-like (LDHs) compounds. The $d_{(0\,0\,3)}$ and $d_{(1\,1\,0)}$ values lead to the interslab

Table 1
Composition and lattice parameters of as prepared hydroxides

	Ni/Co/Mn ratio		*a* (Å)	*c* (Å)
	In solutions	In hydroxides according to chemical analysis		
Sample A-1, *Sample B*-1	0.8/0.1/0.1	0.794/0.101/0.105, 0.792/0.102/0.106	3.124 ± 0.003, ~3.09	4.649 ± 0.007, ~22.6
Sample A-2, *Sample B*-2	0.6/0.2/0.2	0.610/0.195/0.195, 0.608/0.197/0.195	3.066 ± 0.004, ~3.04	4.585 ± 0.007, ~23.0
Sample A-3, *Sample B*-3	0.33/0.33/0.33	0.340/0.321/0.339, 0.345/0.321/0.334	3.215 ± 0.004, ~3.08	4.706 ± 0.011, ~25.2

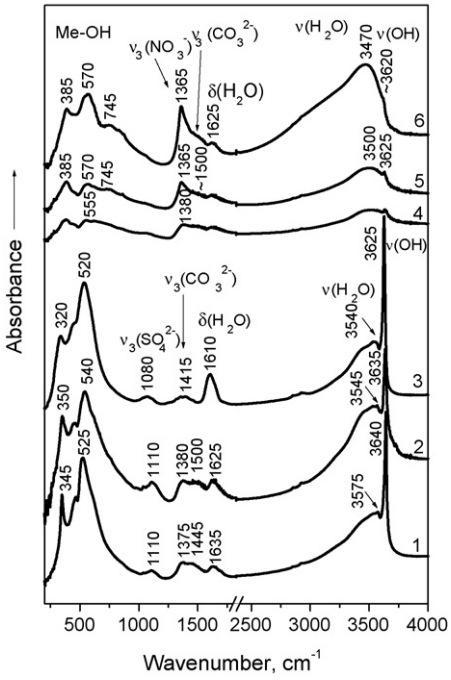

Fig. 2. IR spectra of as prepared mixed Ni–Mn–Co hydroxides: 1, 4: $Ni_{0.8}/Mn_{0.1}/Co_{0.1}$; 2, 5: $Ni_{0.6}/Mn_{0.2}/Co_{0.2}$; 3, 4: $Ni_{0.33}/Mn_{0.33}/Co_{0.33}$; 1–3: *samples A*; 4–6: *samples B*.

distance ($c_{hex.}/3 = d_{(0\,0\,3)}$) and to the metal–metal intraslab distance, respectively. As can be seen from Table 1, parameter *a* has lower values as compared with those for the correspondent *samples A*, while parameter *c* sharply increases. The largest *c* parameter is observed for the $Ni_{1/3}/Co_{1/3}/Mn_{1/3}$ sample with the highest Mn and Co content. The increased interslab distance of *samples B* in comparison with that of *samples A* results from the intercalation of anions and water molecules so as to compensate the excess of positive charge of Mn^{3+} and Mn^{4+} ions within the slab (see below).

X-ray data were confirmed by IR spectroscopy. Vibration modes observed in the IR spectra of *samples A* can be divided into some groups (Fig. 2). The bands in the 300–700 cm^{-1} range are associated with the vibration modes of Me–OH bonds; they are more complicated as compared with the spectra of β-$Ni(OH)_2$ and β-$Ni_{1-x}Co_x(OH)_2$. Narrow and intensive bands at 3575–3640 cm^{-1} are characteristic of isolated OH groups; they shift to higher frequencies with increased Mn and Co content indicating change in Me–OH bond strength: it decreases with bond strength increase. The broad bands at 3400 and 1610–1635 cm^{-1} correspond to stretching and bending vibration modes of water molecules. Low intensive bands at 1375–1445 cm^{-1} and 1080–1100 cm^{-1} characterize vibrations of residual anionic groups: CO_3^{2-} and SO_4^{2-}, respectively.

As can be seen from Fig. 2, IR spectra of *samples B* are significantly different from those of *samples A*. The observed bands are less intensive, but some broader. The bands of the Mn–OH vibration modes shift to higher frequencies, and an additional band above 700 cm^{-1} appears, probably indicating Mn–O vibration mode. The absence of visible bands of the OH stretches in the IR spectra for the samples 4–6 evidences hydrogen bond formation either with interlayer water molecules or with unprotonated oxygen atoms [8]. Note, that such spectra are identical to the spectra of LDHs. The bands, correspondent to intercalated anions (NO_3^- and CO_3^{2-}), become much more intensive with increasing Mn content pointing that larger negative charge is necessary to compensate increased positive charge of the slab.

Thus, according to X-ray and IRS data, two structural types of mixed Ni–Mn–Co hydroxides were obtained using different synthetic conditions. All as prepared *samples A* are characterized preferably by brucite structure, almost consistent with the β-$Me(OH)_2$ (Me = Ni, Co, Mn) structure, with small amounts of water molecules and anions, probably absorbed on the surface (*c* parameter is low), whereas *samples B* possess hydrotalcite-like structure (LDHs) with a large amount of intercalated species. Increased positive charge of the slab due to enhanced oxidation state of Mn ions (>2+) is compensated by anions in the interslab. Most likely, a partial proton loss of hydrogen groups occurs and different β- and α-domains, described for Ni–Mn hydroxides in [6–8], co-exist along *c*-axis. There is no evidence that $Ni_{1-x}Co_x(OH)_2$—layered manganese oxide solid solutions (analogue to asbolanes minerals) [10,ASTM 43-1459] can be prepared by co-precipitation method. However, this requires additional study using single crystals.

3.3. Electronic state of ions

The electronic state of d-ions in *samples A* was studied by XPS which gives information about surface and near-surface ions. To extract the information about chemical states of the elements, the narrow regions of their core level spectra were measured, and the original XPS spectra were decomposed into separate components. The latter procedure involved subtraction of the Shirley background and a curve fitting using the symmetric Doniach–Sunjic functions. Peaks of Al $K\alpha_{3,4}$ X-ray satellites were also taken into account. The quantitative analysis was based on the total areas of the XPS peaks normalized to the literature atomic sensitivity factors [19].

Fig. 3 shows the Ni2p, Mn2p and $Co2p_{1/2}$ core level spectra of the β-(Ni–Mn–Co) hydroxides. Their relative atomic concentrations are shown in Table 2. The Ni2p spectra are characteristic of Ni^{2+} with the $Ni2p_{3/2}$ and $Ni2p_{1/2}$ peaks at 855.5 and 873.1 eV accompanied by so-called shake-up satellites (S_1 and S_2) which are located at ~6 eV above the principal lines (Fig. 3a). Such intensive shake-up satellites are usually observed for paramagnetic nickel (2+) compounds and are attributed to charge transfer multielectron transitions [20–22]. Two extra peaks at 845 and 852 eV correspond to Al $K\alpha_{3,4}$ X-ray satellites from the $Ni2p_{3/2}$ line and from the $MnL_3M_{45}M_{45}$ Auger line. Note, that the major $Ni2p_{3/2}$ peak and the spin-orbital splitting (the difference between $Ni2p_{3/2}$ and $Ni2p_{1/2}$ levels) are in good agreement with those reported for Ni^{2+} in $Ni(OH)_2$ [20,21]. At the same time, a spectrum of Ni_2O_3, for instance, consists of a sharp $Ni2p_{3/2}$ peak at 856.7 eV accompanied by a weak, high-binding-energy satellite centered at 864 eV [22]. Thus, the XPS data indicate that in the β-(Ni–Mn–Co) hydroxides, nickel is present in the Ni^{2+} state.

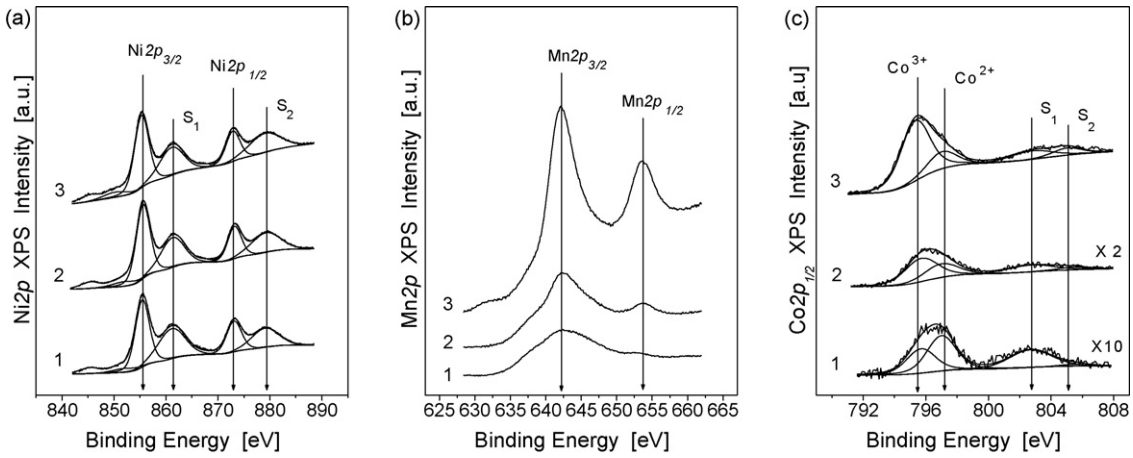

Fig. 3. Ni2p (a), Mn2p (b) and $Co2p_{1/2}$ (c) core level spectra of as prepared mixed β-(Ni–Mn–Co) hydroxides: 1: $Ni_{0.8}/Mn_{0.1}/Co_{0.1}$; 2: $Ni_{0.6}/Mn_{0.2}/Co_{0.2}$; 3: $Ni_{0.33}/Mn_{0.33}/Co_{0.33}$. All spectra were calibrated against C1s line from adventitious carbon (284.8 eV) and were normalized to correspondent Ni2p total intensity.

Unfortunately, the Mn2p region overlaps with a strong Ni $L_2M_{23}M_{45}$ Auger spectrum and the concentration of Mn ions in the surface and near-surface layers is low (Fig. 3b). As a result, it is not possible to make a correct curve-fitting analysis of the Mn2p spectra. Nevertheless, one can see two sharp peaks at 642.3 and 653.7 eV in the $Ni_{0.33}/Co_{0.33}/Mn_{0.33}$ spectrum which corresponds to the $Mn2p_{3/2}$ and $Mn2p_{1/2}$ lines (Fig. 3b). The similar features at 642.4 and 653.8 eV are observed for the $Ni_{0.6}/Co_{0.2}/Mn_{0.2}$ sample. In the $Ni_{0.8}/Co_{0.1}/Mn_{0.1}$ spectrum, one can see intensive photoemission near 642 eV (Ni $L_2M_{23}M_{45}$ Auger spectrum) and only a weak feature at 653.1 eV ascribed to the $Mn2p_{1/2}$ peak. Comparing the observed binding energies with those reported for different Mn-containing oxides [23,24], we suppose that Mn ions in the β-(Ni–Mn–Co) hydroxides are mainly in the 4+ charge state at high Mn contents ($x \geq 0.2$) and in the 3+ charge state at low Mn contents ($x = 0.1$).

To identify the chemical state of cobalt ions, we used the $Co2p_{1/2}$ spectrum only, because the $Co2p_{3/2}$ region overlaps with a strong Ni $L_3M_{23}M_{23}$ Auger spectrum [19]. The peak fitting procedure reveals a superposition of four features in the $Co2p_{1/2}$ spectra (Fig. 3c). According to previous XPS studies [25–27], the $Co2p_{3/2}$ binding energies for different cobalt oxides (CoO, Co_3O_4, CoOOH) are close to each other, thus, the secondary features should be used for analysis such as satellites, spin-orbital splitting and $Co2p_{1/2}$ binding energy. For example, cobalt (2+) compounds exhibit well-defined shake-up satellite structure and high values of Co2p spin-orbital splitting in the 15.5–16.0 eV range. On the contrary, cobalt (3+) compounds, as well as metallic cobalt, exhibit both spin-orbital splitting, usually close to 15 eV, and weak satellites. In the first case, the shake-up satellites are observed at the energy of 5–6 eV higher than the principal $2p_{3/2-1/2}$ doublet, while in the second case, they are observed at 10–11 eV above the principal lines. Based on the analysis above, the features at 795.3–795.7 and 805.0–805.4 eV ($Co2p_{1/2}$ principal line and shake-up satellites, respectively) can be assigned to Co^{3+} ions, while the features at 797.0 and 802.8 eV to Co^{2+} ions (Fig. 3c). It should be noted that the binding energy of the second $Co2p_{1/2}$ line (797.0 eV) is very close to that observed for $Co(OH)_2$ [25]. For $LiCoO_2$, we detected the $Co2p_{1/2}$ line at 795.0 eV [27]. Thus, our XPS analysis shows that Co in the hydroxides under study exists in two different oxidation states, namely Co^{2+} and Co^{3+}. The relative amount of Co^{3+} ions increases with Co content (Table 2).

According to the XPS analysis, the surface and near surface chemistry of the hydroxides differs from chemical composition shown in Table 1. First of all, the samples under study are characterized by excess oxygen content (see Table 2). One of the reasons could be the presence of carbonates on the surface [26,27]. Indeed, two features at 284.8 and 288.7 eV were detected in the C1s spectra. The first one, more intensive, corresponds to carbon in hydrocarbon impurities [28], while the second one—to carbon in carbonate groups. The analysis of relative intensity of the second C1s feature indicates that only ~10% of oxygen belongs to carbonates.

We observed a strong effect of nickel segregation (see Table 2) and suggested that some Ni-rich oxide is formed on the sur-

Table 2
Binding energies (eV), atomic ratios and Co^{2+}/Co^{3+} percentage for as prepared mixed β-(Ni–Mn–Co) hydroxides

	$Ni_{0.8}/Co_{0.1}/Mn_{0.1}$	$Ni_{0.6}/Co_{0.2}/Mn_{0.2}$	$Ni_{0.33}/Co_{0.33}/Mn_{0.33}$
$Ni2p_{3/2}/Ni2p_{1/2}$	855.5/873.2	855.7/873.3	855.4/873.0
$Mn2p_{3/2}/Mn2p_{1/2}$	–/653.1	642.4/653.8	642.3/653.7
$Co2p_{1/2}$ (Co^{2+}/Co^{3+})	797.0/795.7	797.0/795.7	797.0/795.3
[Mn]/[Ni]	0.02	0.14	0.78
[Co]/[Ni]	0.03	0.10	0.50
Co^{2+}/Co^{3+}	52/48	47/53	29/71
[O]/[Ni + Co + Mn]	2.5	3.0	3.6

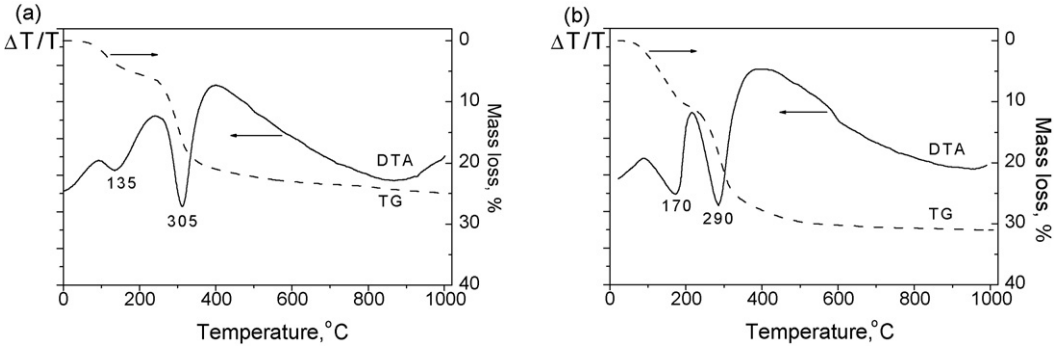

Fig. 4. DTA- and TG-curves of as prepared β- (a) and α-$Ni_{0.8}/Mn_{0.1}/Co_{0.1}$ (b) hydroxides.

face. Indeed, in the O1s spectra of the $Ni_{0.8}/Co_{0.1}/Mn_{0.1}$ and $Ni_{0.6}/Co_{0.2}/Mn_{0.2}$ samples, two features which correspond to oxygen in different chemical settings are present. The main peak at 530.9 eV is ascribed to OH groups in the lattice of hydroxides. The subpeak at 529.6 eV can be attributed to the presence of some metal oxide on the surface. For example, the O1s binding energies for NiO, CoO, Co_2O_3 are observed in the 529.6–529.9 eV range [20]. In contrast, in the O1s spectrum of the $Ni_{0.33}/Co_{0.33}/Mn_{0.33}$ hydroxide, only wide symmetric peak at 530.4 eV is present corresponding to hydroxyl groups.

Thus, XPS study shows that Ni/Co/Mn hydroxides are mixed-valence compounds where Ni ions are in 2+ oxidation state, whereas Mn and Co ions are in 3+/4+ and 2+/3+, respectively; their oxidation state increases with an increase of their content. Note, that according to XPS study, oxidation state of Ni, Co and Mn in $LiNi_{1/3}Co_{1/3}Mn_{1/3}O_2$ cathode was also found to be 2+, 3+ and 4+, respectively.

3.4. Thermal decomposition

According to TG- and DTA-analysis, as prepared materials decompose in two stages as a result of dehydration and dehydroxylation. The process is accompanied by two endothermic effects (Fig. 4). The first stage is observed in the 50–200 °C range for *samples A* and in the 100–200 °C range for *samples B*. Since parameter *c* for *samples A* is rather small, mass loss is most probably corresponds to release of weakly bounded adsorbed water, whereas interlayer water is partly released from *samples B*. The second stage of decomposition is observed in the 200–400 °C range with the peak temperature increasing for the $Ni_{0.33}/Mn_{0.33}/Co_{0.33}$ sample. It is mainly associated with dehydroxylation of hydroxide layers and decomposition of interlayer anions [29,30]. Mass loss is decreased with increased Mn content for *samples A* and *B* indicating the decreased amount of OH groups. However, any calculation based on weight loss leads to uncertainty in determination of the content of interlayer molecular water, hydroxide and anion groups because of overlapping of dehydration, dehydroxylation, decarbonization, etc., processes. Interestingly, that the heating of pure $Co(OH)_2$ is accompanied by exothermic effect due to the following redox reactions

$$Co(OH)_2 \rightarrow CoOOH \rightarrow Co_3O_4.$$

As prepared hydroxides were heated at 400 and 700 °C. After heating at 400 °C broad reflections of NiO bunsenite and $(Ni,Mn,Co)_3O_4$ spinel were observed on the XRD patterns independent of Ni/Mn/Co ratio (Fig. 5a). The amount

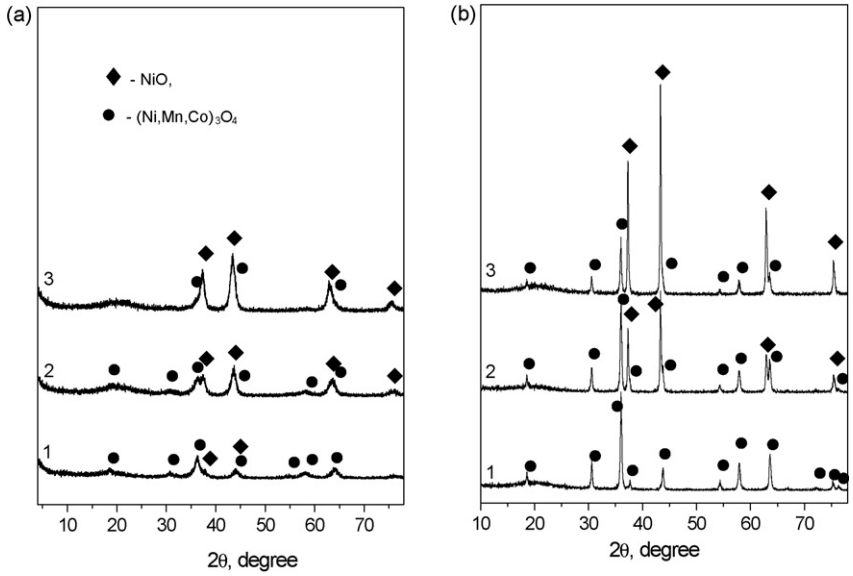

Fig. 5. X-Ray patterns of the decomposition products: *a* = 400 °C; *b* = 700 °C. 1: β-$Ni_{0.33}/Mn_{0.33}/Co_{0.33}$, 2: β-$Ni_{0.6}/Mn_{0.2}/Co_{0.2}$ and 3: β-$Ni_{0.8}/Mn_{0.1}/Co_{0.1}$.

of NiO is sharply decreased from $Ni_{0.8}/Mn_{0.1}/Co_{0.1}$ to $Ni_{0.33}/Mn_{0.33}/Co_{0.33}$ samples while that of spinel (most probably, $MnCo_2O_4$) is increased. According to [31], this spinel is partially inversed, i.e., Co^{2+} and Mn^{3+} ions are distributed between tetra- and octa-positions. This means that under heating, reduction processes occur. The composition of the spinels must vary versus Ni/Mn/Co ratio in initial hydroxides.

The same two phases, NiO and spinel, are present on the XRD patterns of the products obtained at 700 °C (Fig. 5b). Their reflections become narrow and more intensive. For the $Ni_{0.33}/Mn_{0.33}/Co_{0.33}$ sample, practically homogeneous high-dispersed $(Ni,Mn,Co)_3O_4$ spinel with $a = 8.274 \pm 0.001$ Å is formed. We did not observe the formation of Ni_6MnO_8 with murdochite type structure and $NiMnO_3$ with ilmenite structure as intermediate products of the Ni–Mn LDHs decomposition published in [29,30].

4. Conclusion

Thus, it has been shown that varying conditions of co-precipitation processes, one can prepare mixed Ni–Mn–Co hydroxides with different crystal structure: either brucite, or hydrotalcite-like (LDHs). According to XPS study, Ni–Mn–Co hydroxides are mixed-valence compounds. Only Ni ions are in 2+ oxidation state, while Mn and Co ions are in 3+/4+ and 2+/3+ state, respectively. The surface and near surface chemistry of the hydroxides differs from that of the bulk. For Ni-rich hydroxides, a strong effect of nickel segregation and carbonization is observed. Mixed Ni–Mn–Co hydroxides decompose in two steps resulting in formation of NiO and $(Ni,Mn,Co)_3O_4$ spinel. The latter one prepared at moderate temperature is high dispersed and probably should posses promising catalytic activity.

Acknowledgement

This work was financially supported by the Russian Foundation for Basic Research (grant 05-03-32703).

References

[1] P. Oliva, J. Leonardi, J.F. Laurent, C. Delmas, J.J. Braconnier, M. Figlarz, F. Fievet, J. Power Sources 8 (1982) 229.
[2] P.V. Kamath, G.H.A. Therese, J. Gopalakrishnan, J. Solid State Chem. 128 (1997) 38.
[3] P.V. Kamath, M. Dixit, L. Indira, A.K. Shukla, V.G. Kumar, N. Munichandraiah, J. Electrochem. Soc. 141 (1994) 2956.
[4] C. Faure, C. Delmas, M. Fouassier, P. Willmann, J. Power Sources 35 (1991) 249.
[5] L. Demourgues-Guerlou, J.J. Braconnier, C. Delmas, J. Solid State Chem. 104 (1993) 359.
[6] R.S. Jayashree, P.V. Kamath, J. Power Sources 107 (2002) 120.
[7] L. Guerlou-Demourgues, C. Denage, C. Delmas, J. Power Sources 52 (1994) 269.
[8] L. Guerlou-Demourgues, C. Delmas, J. Power Sources 52 (1994) 275.
[9] A. Vaccari, Catal. Today 41 (1998) 53.
[10] Y. Xu, Q. Feng, K. Kajiyoshi, K. Yanagisawa, Chem. Mater. 14 (2002) 697.
[11] N. Yabuuchi, T. Ohzuku, J. Power Sources 119–121 (2003) 171.
[12] J. Cho, T.-J. Kim, J. Kim, M. Noh, B. Park, J. Electrochem. Soc. 151 (2004) A1899.
[13] Y. Chen, G.X. Wang, K. Konstantinov, H.K. Liu, S.X. Dou, J. Power Sources 119–121 (2003) 184.
[14] P.Y. Liao, J.G. Duh, S.R. Sheen, J. Electrochem. Soc. 152 (2005) A1695.
[15] Z. Liu, A. Yu, J.Y. Lee, J. Power Sources 81/82 (1999) 416.
[16] J. Jiang, K.W. Eberman, L.J. Krause, J.R. Dahn, J. Electrochem. Soc. 152 (2005) A1879.
[17] S. Jouanneau, J.R. Dahn, Chem. Mater. 15 (2003) 495.
[18] M.-Y. Lee, Y.-J. Kang, S.-T. Myung, Y.-K. Sun, Electrochim. Acta 50 (2004) 939.
[19] C.D. Wagner, W.M. Riggs, L.E. Davis, J.F. Moulder, G.E. Muilenberg (Eds.), Handbook of X-Ray Photoelectron Spectroscopy, Perkin-Elmer, Eden Prairie, Minnesota, 1978.
[20] N.S. McIntyre, M.G. Cook, Anal. Chem. 47 (1975) 2208.
[21] C.P. Li, A. Proctor, D.M. Hercules, Appl. Spectr. 38 (1984) 880.
[22] A.F. Carley, S.D. Jackson, J.N. O'Shea, M.W. Roberts, Surf. Sci. 440 (1999) L868.
[23] M. Oku, K. Hirokawa, S. Ikeda, J. Electron Spectrosc. Relat. Phenom. 7 (1975) 465.
[24] A.A. Audi, P.M.A. Sherwood, Surf. Interface Anal. 33 (2002) 274.
[25] Z. Zsoldos, L. Guczi, J. Phys. Chem. 96 (1992) 9393.
[26] A.A. Khassin, T.M. Yurieva, V.V. Kaichev, V.I. Bukhtiyarov, A.A. Budneva, E.A. Paukshtis, V.N. Parmon, J. Mol. Catal. A. 175 (2001) 189.
[27] N.V. Kosova, V.V. Kaichev, V.I. Bukhtiyarov, D.G. Kellerman, E.T. Devyatkina, T.V. Larina, J. Power Sources 119–121 (2003) 669.
[28] R. Alcantara, G.F. Ortiz, P. Lavela, J.L. Tirado, W. Jaegermann, A. Thißen, J. Electroanal. Chem. 584 (2005) 147.
[29] C. Barriga, J.M. Fernandez, M.A. Ulibarri, F.M. Labajos, V. Rives, J. Solid State Chem. 124 (1996) 205.
[30] F. Kovanda, T. Grygar, V. Dornicak, Solid State Sci. 5 (2003) 1019.
[31] A.V. Salker, S.M. Gurav, J. Mater. Sci. 35 (2000) 4713.